Onset of Asian desertification by 22 Myr ago inferred from loess deposits in China

Z. T. Guo*, William F. Ruddiman†, Q. Z. Hao*, H. B. Wu*, Y. S. Qiao*, R. X. Zhu*, S. Z. Peng*, J. J. Wei*, B. Y. Yuan* & T. S. Liu*

** Institute of Geology and Geophysics, Chinese Academy of Sciences, PO Box 9825, Beijing 100029, China*
† Department of Environmental Science, Clark Hall, University of Virginia, Charlottesville, Virginia 22903, USA

The initial desertification in the Asian interior is thought to be one of the most prominent climate changes in the Northern Hemisphere during the Cenozoic era[1–4]. But the dating of this transition is uncertain, partly because desert sediments are usually scattered, discontinuous and difficult to date. Here we report nearly continuous aeolian deposits covering the interval from 22 to 6.2 million years ago, on the basis of palaeomagnetic measurements and fossil evidence. A total of 231 visually definable aeolian layers occur as brownish loesses interbedded with reddish soils. This new evidence indicates that large source areas of aeolian dust and energetic winter monsoon winds to transport the material must have existed in the interior of Asia by the early Miocene epoch, at least 14 million years earlier than previously thought[3,5]. Regional tectonic changes and ongoing global cooling are probable causes of these changes in aridity and circulation in Asia.

Uplift of the Himalayan–Tibetan plateau[1–3] and changes in land–sea distribution[4] have been invoked as driving forces behind long-term Cenozoic climate deterioration. One problem in understanding these links is defining the timing of major tectonic and climatic changes, including the onset and development of aridification in Asia. Continuous long-term records with well constrained chronologies are especially important.

Desert loess is particularly valuable as an indicator of dryland evolution because sizeable deserts are needed as sources for aeolian deposits[5–7]. As a result, most studies focus on regions which receive wind-blown sediments produced in or near deserts. In northern China, nearly half a million square kilometres are covered by aeolian deposits[7].

The well known loess–soil sequences of the last 2.6 million years (Myr) contain more than thirty major soil units interbedded with loess[7,8]. These are underlain at some localities in the eastern Loess plateau by the Hipparion Red-Earth Formation (also called Red Clay)[3,5,9–11]. Palaeomagnetic measurements date the lower boundary of the Red-Earth Formation to ~7–8 Myr ago[9,10]. Detailed studies confirm that at least the portion of this sequence younger than 6.2 Myr is of aeolian origin[5]. This places the minimum age of initiation of sizeable deserts in Asia in the late Miocene[3,5].

Thick silty deposits with numerous palaeosols are also widely distributed in the western loess region, an area between the Liupan mountains and the Tibetan plateau, representing one-fifth of the area of the Loess plateau (Fig. 1). Neither the origin nor stratigraphy of these layers has been investigated in detail. The sequences reported here were found in Qinan county (Gansu province), about 160 km northeast of the Tibetan plateau and about 300 km south of the Tengger desert (Fig. 1). The present-day climate at Qinan is semi-arid with a mean annual rainfall of 400 mm and an annual mean temperature of 10.4 °C.

The region has experienced strong erosion, and its topography is characterized by valleys flanked by elongated hills with thick and relatively flat sedimentary sequences deposited on metamorphic bedrock of early Palaeozoic age. At the bottom of the sedimentary sequences lies a waterlain deposit 10–30 m thick, consisting of reddish clay and containing abundant stratified sandy layers and bedrock fragments. Hill tops are unconformably mantled by pale-brown Quaternary-period loess up to 30 m thick. In between lies the Miocene loess sequence reported here.

The most complete loess sequence (QA-I) (105° 27′ E, 35° 2′ N) is 253.1 m in thickness and located 27 km northwest of Qinan city (Fig. 1), and a second section (QA-II, 220.6 m thick) is located 2 km from QA-I. QA-I contains 231 visually definable reddish layers interbedded with yellow-brown or brown silty layers, all nearly horizontal (Fig. 2). This layering is reflected in variations of magnetic susceptibility (Fig. 3), with higher values in red layers than in surrounding silty units. According to field lithostratigraphic correlation, the top part of QA-II was truncated by erosion. A spatially correlative erosion surface was observed at a depth of 59.8 m in QA-I and 20.0 m in QA-II.

The reddish layers have a silty clay or clay texture and moderate to strong angular blocky or prismatic structure, characteristic of soils[12]. The abundant biological pores and clay coatings (Fig. 2) observed in microscopic thin sections confirm that these red beds are palaeosols, many of them composite soils. Fine-grained ferrimagnetic minerals of pedogenic origin may be responsible for their higher susceptibility values, as in Quaternary loess–soil sequences in China[13].

Most soils are underlain by carbonate nodule horizons similar to those in Quaternary loess[14]. The non-palaeosol silty layers have a yellow-brown or brown colour and massive structure. Thin-section examination shows that the coarse fraction (>10 μm) is dominated by quartz (50–60%) and feldspar and mica (>30%). All mineral grains have angular shapes with no significant rounding (Fig. 2). The grain size is generally finer than 70 μm with the <20 μm fraction amounting to approximately 80%. The field aspects, mineral assemblage, grain morphology and grain-size distribution are characteristic of aeolian dust deposits[6,7,15]. This is also confirmed

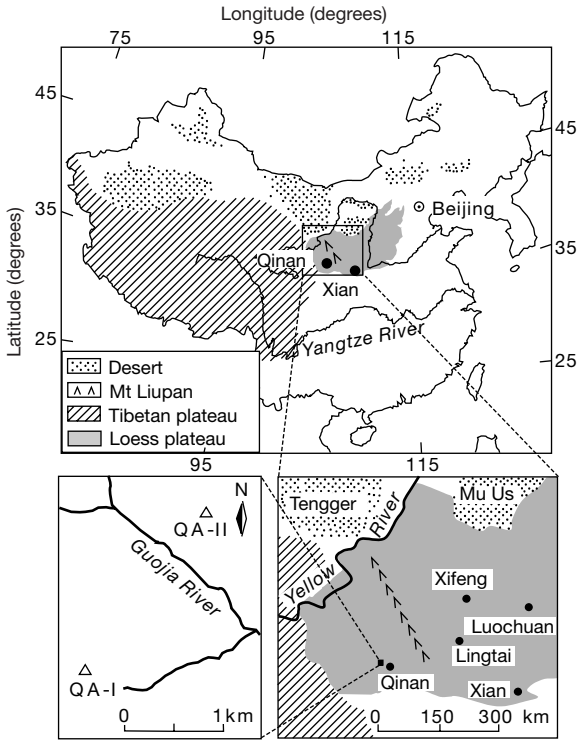

Figure 1 Maps showing the Loess plateau, Tibetan plateau, deserts in northern China and location of sites studied.

by the high degree of geochemical similarity to the Quaternary loess (Fig. 2).

Micromammalian fossils at Site QA-I were examined to determine the approximate age of the sequence. The seven fossil assemblages (Table 1) indicate ages from early Miocene to late Miocene[16–20]. Palaeomagnetic measurements were made on both the QA-I and AQ-II sections. After removing the secondary viscous remanent magnetization, clear polarity zonations were obtained (Fig. 3). The magnetozones of QA-I correlate with polarity intervals C6An.2n to C3An.2n in the geomagnetic polarity timescale (GPTS)[21], and only C5n.1n and C5n.1r are missing from the sequence. The lack of these polarity intervals in QA-I, and of polarity intervals C4Ar.1r to C5n.1r in QA-II, is attributable to the erosion surfaces in both sections. This erosional break occurred around 9–10 Myr ago.

Extrapolation of the prevailing accumulation rate below the oldest geomagnetic boundary yields a basal age of about 22 Myr for the QA-I section. The polarity zones below the erosion surface at a depth of 20.0 m in QA-II are correlative with C5n.2n to C6An.2n and give a basal age of about 21.6 Myr. The chronology obtained from magnetostratigraphy is consistent with the fossil assemblages (Table 1).

In summary, palaeomagnetic measurements date the main Qinan sections from around 22 to 6.2 Myr ago, except for hiatuses spanning around 0.7 Myr in QA-I and 1.2 myr in QA-II. This gives an average dust accumulation rate at QA-I of approximately 1.67 cm kyr^{-1}. With 231 soils and aeolian layers visible in a sequence covering 15.1 Myr (after accounting for the hiatus), the average duration of each loess–soil pair in QA-I is 65,000 years, within the bandwidth typical of orbital-scale variations[22]. In summary, we have clear evidence that a baseline shift in Asian climate occurred by at least 22 Myr ago, and that aeolian sediments began to be deposited

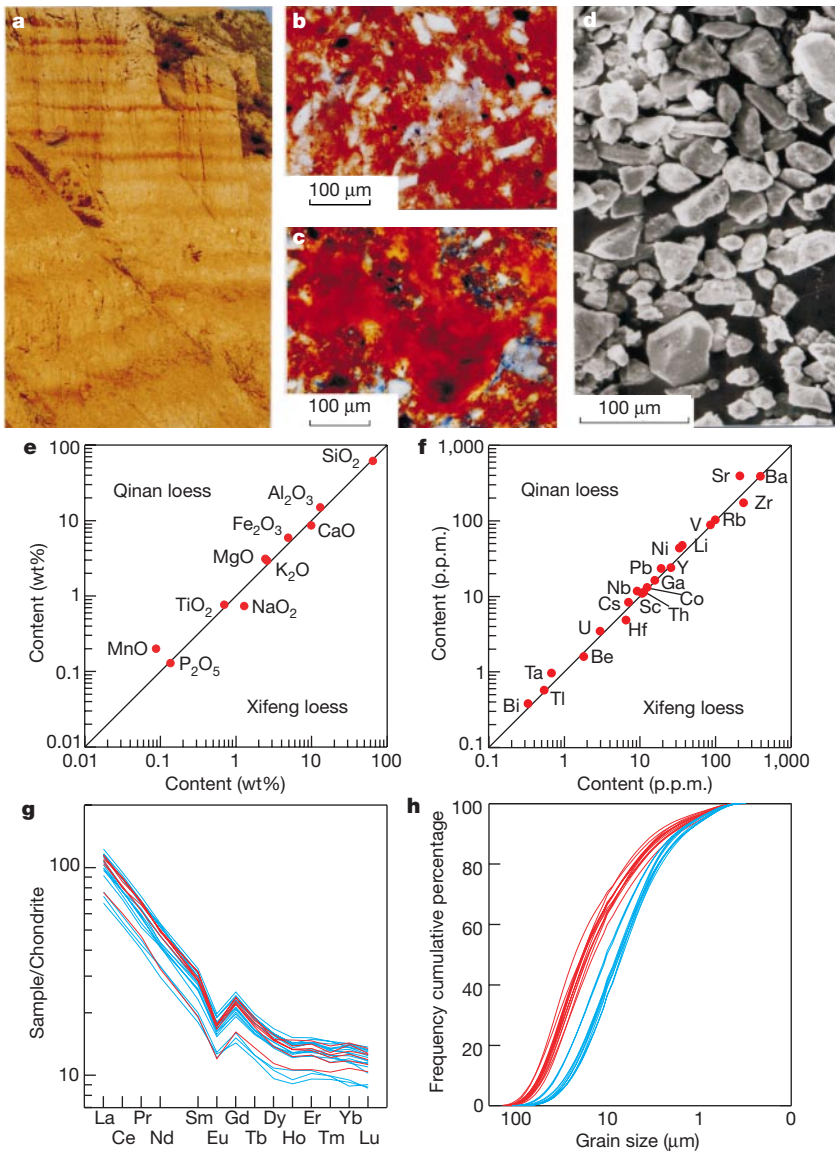

Figure 2 Morphological, geochemical and sedimentological properties of the Qinan aeolian deposits. **a**, Field picture showing the alternation of loess (yellow-brown layers) and palaeosols (reddish layers). **b**, Microscopic image showing the groundmass of a palaeosol. **c**, Microscopic image showing the clay coatings in palaeosols. **d**, Angular morphology of quartz grains under scanning electron microscope. **e**, **f**, Comparison of major and trace element compositions between the Qinan aeolian deposits (average of 16 samples from QA-I) and Quaternary loess from Xifeng (average of 6 samples). **g**, Comparison of rare-earth elemental (REE) distribution patterns between the Qinan aeolian deposits (blue lines) and the Quaternary Xifeng loess (red lines). **h**, Grain-size distributions of the Qinan aeolian deposits (blue lines) and the Quaternary Xifeng loess (red lines).

on the loess plateau with orbital-scale cyclicity.

Loess deposits require both a sizeable source area arid enough to create aeolian particles and an atmospheric circulation sufficiently energetic to carry the particles from the deserts to the points of deposition. The high degree of geochemical similarity between the Miocene and the Quaternary loesses (Fig. 2) suggests similar sources for the dust. Quaternary dust deposits in northern China mainly originated from the desert lands in the north and northeast[3,7,23]. By analogy, the Qinan aeolian sequences provide firm evidence that deserts large enough to produce aeolian dust must have been formed at or by 22 Myr ago in central Asia, some fourteen million years earlier than previously thought[3,5,9–11].

The Quaternary loess was probably carried from central Asia to the Loess plateau by northwesterly winds in the Asian winter monsoon. Today, strong northwesterly winds occur in the eastern portion of the high-pressure cell over Siberia[3,7]. The Qinan deposits indicate that a winter wind pattern similar to the modern Asian winter monsoon had formed by the early Miocene. However, the finer texture of the Qinan loess compared with the Quaternary loess deposits (Fig. 2) suggests weaker wind strength and smaller extent of deserts. The alternations between loess and reddish soils indicate cyclical changes in intensity of winter and summer monsoons.

Three tectonic-scale changes, two regional in scope and one global, are probably causes of these joint changes in aridity and circulation. Interiors of large continents are normally arid because of the great distance to ocean moisture sources, but sediments deposited in the western Loess plateau of East Asia were fluvial-lacustrine through the Oligocene epoch[24]. One source of Oligocene moisture in the Asian interior may have been the broad Paratethys sea in western-central Asia[4]. As this inland sea shrank during the late Oligocene and early Miocene, it would have left the Asian interior more arid and would also have intensified the continentality, with hotter summers and colder winters. The onset of greater aridity recorded by the early Miocene loess is broadly consistent with this change in land–sea distribution.

A second regional-scale factor was uplift of the Tibetan–Himalayan complex, which began at smaller scales by 40 Myr ago[25], but intensified 25 to 20 Myr ago in the Himalayas, and southern Tibetan plateau[26]. Geological evidence indicates rapid surface exposure and erosion of deeply buried rocks and minerals shortly after cooling. Because extremely rapid erosion only occurs in regions of high relief, this evidence indicates that sizeable parts of the south Tibetan–Himalayan complex were elevated by 25 to 20 Myr ago[26].

General circulation model experiments reveal the probable effects of large-scale Tibetan–Himalayan uplift on Asian climate[1–3]. Uplift strengthens the summer monsoon and brings wetter climates to India and southeast Asia, but this moisture cannot reach the Asian interior because uplifted Himalayan topography blocks flow from the south. As a result, central Asia becomes drier as uplift proceeds. Uplift also produces drier climates in central Asia in the winter season because dry winter monsoon winds blow out of the Asian interior. The combination of summer and winter drying produces year-round aridity and forms deserts. In addition, uplift strengthens the flow of winter monsoon winds from the northwest. These model simulations[1–3], combined with geological evidence[26], provide an explanation for the early Miocene loess deposits: the southern margin of the Tibetan plateau was sufficiently elevated by 22 Myr ago to cause year-round drying and desert formation in the Asian interior and to produce northwest winds strong enough to carry aeolian particles southeast into the Loess plateau.

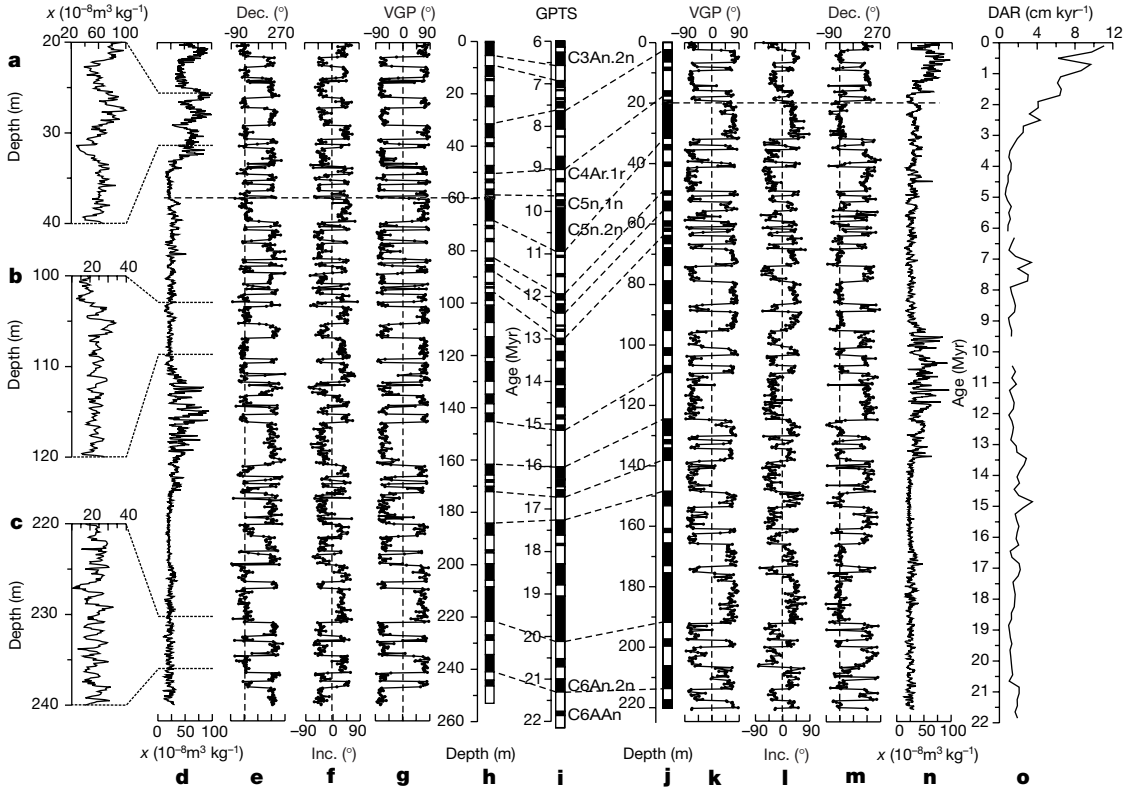

Figure 3 Magnetostratigraphy and magnetic susceptibility of the Qinan aeolian sequences and late Cenozoic dust accumulation rate in northern China. **a**–**h**, Profiles of magnetic susceptibility (χ), declination (Dec.), inclination (Inc.), virtual geomagnetic pole latitudes (VGP) and polarity zonation of QA-I. **i**, Reference geomagnetic polarity timescale (GPTS)[21]. **j**–**n**, Polarity zonations, VGP, Inc., Dec. and susceptibility profiles of QA-II. **o**, Dust accumulation rate (DAR) in northern China. Data for 0–6.2 Myr interval are calculated based on the loess–soil sequence and the Hipparion Red-Earth formation at Xifeng. The 6.2–22.0 Myr portion is based on QA-I. Calculation was made at 200,000-year intervals. The timescales are obtained using geomagnetic boundaries (refs 8, 9 for Xifeng) as age controls and then interpolating, using the magnetic susceptibility age model for loess[8]. Horizontal discontinuous lines indicate the erosion surfaces in both sections.

Table 1 Micromammalian fossil assemblages from the QA-I section

Depth (m)	Assemblage	Fossils	Depth (m)	Assemblage	Fossils
8	A1	*Alilepus* cf. *A. annectens*	197	A5	*Ansomys* sp.
		Ochotona sp.			*Atlantoxerus* sp.
		Pararhizomys sp.			*Sayimys minor*
		Prosiphneus licenti			*Sinolagomys* cf. *S. ulungurensis*
36	A2	*Ochotona* sp.			*Sinolagomys* sp.
		Prosiphneus n. sp.1			Tachyoryctoididae gen. et sp. indet.
82	A3	*Prosiphneus* n. sp.2	220	A6	*Distylomys* cf. *D. qianlishanensis*
		Sciuridae gen. et sp. indet.			*Distylomys* cf. *D. tedfordi*
148	A4	*Alloptox gobiensis*			*Litodonomys* sp.
		Ansomys sp.			*Prodistylomys* cf. *P. xinjiangensis*
		Cricetodon sp.			*Sinolagomys* cf. *S. kansuensis*
		Desmatolagus sp.			*Sinolagomys* cf. *S. ulungurensis*
		Gobicricetodon sp.	227	A7	Ansomyinae gen. et sp. indet.
		Mioechinus sp.			*Distylomys* sp.
		Talpidae gen. et sp. indet.			*Litodonomys* sp.
					Tachyoryctoididae gen. et sp. indet.

The dominance of *Prosiphneus licenti* in A1 is characteristic of the late Miocene in China[16] and was correlated to MN12 (8.2–7.1 Myr) in the European Neogene Mammal Chronology (ENMC)[17]. A4 is highly similar to the Tunggur fauna in China[18], correlative with MN7-8 (12.5–11.2 Myr) in the ENMC. A5 is characteristic of the early Miocene in China[19]. *Sayimys minor* was geomagnetically dated in the Murree Formation in Pakistan to 18 Myr (ref. 20). A6 and A7 contain species that are abundant in the late Oligocene to early Miocene strata in northern China[19].

Ongoing global cooling during the Cenozoic probably also contributed to regional changes in Asia. Although neither ice sheets nor extensive sea ice appeared in the Northern Hemisphere until late in the Miocene[27], climatic cooling had caused Palaeocene evergreen forests and Eocene-epoch deciduous forests along the Arctic margins to yield to mixed coniferous forests by the early Miocene[28]. Oxygen-isotopic values from benthic foraminifers also indicate significant early Miocene cooling of polar oceans[29]. Cooler high-latitude oceans provide less moisture to continental interiors, promoting continentality at the expense of temperate climates. Continental climates are also generally marked by colder, drier winters with stronger winds.

The Miocene sequences of Qinan do not show any obvious long-term intensification of loess deposition between 22 and 6.2 Myr. The major increases occur after about 3.5 Myr, in the Pliocene and Pleistocene epochs (Fig. 3). This suggests that the level of aridity and the strength of the winter monsoon winds in central Asia remained at moderate levels through the Miocene. Two intervals with higher dust accumulation rates are observed at 15–13 Myr and 8–7 Myr ago. The latter matches independent evidence reported from studies of North Pacific aeolian fractions[30]. Because these intervals of higher aeolian deposition were not sustained, they may simply represent temporary instabilities of climate or land–surface conditions in the dust source region.

The early-Miocene climatic changes reported here intensified in the late Miocene and the Pliocene–Pleistocene, as part of the ongoing deterioration of Cenozoic climate. As sea ice expanded across the Arctic Ocean and ice sheets periodically formed in North America and northern Eurasia, the earlier Miocene trend towards a drier and windier climate in central Asia intensified (Fig. 3). Thick, well defined loess sequences eventually formed in the Loess plateau[5,7,8], replacing the thinner and finer-grained aeolian Miocene deposits reported here. □

Methods

Major chemical elements were analysed by X-ray fluorescence using a Philips PW-1400 unit with analytical uncertainties of 2% for all the major elements except for P_2O_5 and MnO (up to 10%). Trace and rare earth elements were digested with a $HF + HClO_4 + HNO_3$ mixture in Teflon bombs and analyses were made on a Finnigan MAT inductively coupled plasma mass spectrometry (ICP-MS) unit, which gave a precision of less than 10%. Grain-size distribution was determined using a Master Sizer 2000 laser unit.

Magnetic susceptibility was measured on air-dried samples as 10-cm intervals using a Bartington susceptibility meter. Palaeomagnetic measurements were made on 947 samples from QA-I and 846 samples from QA-II at 25–30-cm intervals in the Paleomagnetism Laboratory of the Institute of Geology and Geophysics, Chinese Academy of Sciences. Stepwise thermal demagnetization was performed on 661 samples from QA-1 at an average interval of 40 cm. Samples were demagnetized in a MMTD-600 Thermal Demagnetiser and measured using a 2 G three-axis cryogenic magnetometer, both installed in field-free space. Because stepwise thermal demagnetization on 661 samples from QA-I showed that most of the samples yield a stable characteristic remanent magnetization (ChRM) above 350 °C (see Supplementary Information), the other 286 samples from QA-I and all the samples from QA-II were then demagnetized at 350 and 400 °C. 874 (92%) samples from QA-I and 771 (91%) samples from QA-II gave reliable characteristic remanence directions. Details of the rock magnetic properties will be described elsewhere.

Received 27 September 2001; accepted 16 January 2002.

1. Ruddiman, W. F. & Kutzbach, J. E. Forcing of late Cenozoic northern hemisphere climate by plateau uplift in southern Asia and the American West. *J. Geophys. Res.* **94,** 18409–18427 (1989).
2. Manabe, S. & Broccoli, A. J. Mountains and arid climates of middle latitudes. *Science* **247,** 192–195 (1990).
3. An, Z. S., Kutzbach, J. E., Prell, W. L. & Porter, S. C. Evolution of Asian monsoons and phased uplift of the Himalaya–Tibetan plateau since Late Miocene times. *Nature* **411,** 62–66 (2001).
4. Ramstein, G., Fluteau, F., Besse, J. & Joussaume, S. Effect of orogeny, plate motion and land-sea distribution on Eurasian climate change over the past 30 million years. *Nature* **386,** 788–795 (1997).
5. Guo, Z. T., Peng, S. Z., Hao, Q. Z., Biscay, P. E. & Liu, T. S. Origin of the Miocene-Pliocene Red-Earth formation at Xifeng in northern China and implications for paleoenvironments. *Palaeogeogr. Palaeoclimatol. Palaeoecol.* **170,** 11–26 (2001).
6. Whalley, W. B., Marshall, J. R. & Smith, B. J. Origin of desert loess from some experimental observations. *Nature* **300,** 433–435 (1982).
7. Liu, T. S. *Loess and the Environment* (China Ocean, Beijing, 1985).
8. Kukla, G., An, Z. S., Melice, J. L., Gavin, J. & Xiao, J. L. Magnetic susceptibility record of Chinese loess. *Trans. R. Soc. Edinb. Earth Sci.* **81,** 263–288 (1990).
9. Sun, D. H., An, Z. S., Shaw, J., Bloemendal, J. & Sun, Y. B. Magnetostratigraphy and paleoclimatic significance of Late Tertiary aeolian sequences in the Chinese Loess Plateau. *Geophys. J. Int.* **134,** 207–212 (1998).
10. Sun, D. H., Shaw, J., An, Z. S., Chen, M. Y. & Yue, L. P. Magnetostratigraphy and paleoclimatic interpretation of a continuous 7.2 Ma late Cenozoic eolian sediments from the Chinese Loess Plateau. *Geophys. Res. Lett.* **25,** 85–88 (1998).
11. Ding, Z. L. *et al.* Wind-blown origin of the Pliocene red clay formation in the central Loess Plateau, China. *Earth Planet. Sci. Lett.* **161,** 135–143 (1998).
12. Duchaufour, Ph. *Pédologie Tome 1 Pédogenèse et Classification* (Masson, Paris/New York/Barcelone/Milan, 1983).
13. Maher, B. A. Characterization of soils by mineral magnetic measurements. *Phys. Earth Planet. Inter.* **42,** 76–92 (1986).
14. Guo, Z. T. *et al.* Climate extremes in loess of China coupled with the strength of deep-water formation in the North Atlantic. *Glob. Planet. Change* **18,** 113–128 (1998).
15. Pye, K. & Sperling, C. H. B. Experimental investigation of silt formation by static breakage processes: the effect of temperature, moisture and salt on quartz dune sand and granitic regolith. *Sedimentology* **30,** 49–62 (1983).
16. Zheng, S. H. in *Rodent and Lagomorph Families of Asian Origins and Diversification* (eds Tomida, Y., Li, C. K. & Setoguchi, T.) 57–76 (National Science Museum Monographs 8, Tokyo, 1994).
17. Mein, P. in *European Neogene Mammal Chronology* (eds Lindsay, E. H., Fahlbusch, V. & Mein, P.) 73–90 (NATO ASI Series A 180, Plenum, New York, 1990).
18. Qiu, Z. D. *Middle Miocene Micromammalian Fauna from Tunggur, Nei Mongol* (Science, Beijing, 1996).
19. Qiu, Z. X., Xu, W. Y. & Qiu, Z. D. in *The Miocene Land Mammals of Europe* (eds Rössner, G. & Heissig, K.) 443–455 (Pfeil, München, 1999).
20. Bruijn, H., Hussain, S. T. & Leinders, J. J. M. Fossil rodents from the Murree formation near Banda Daud Shah, Kohat, Pakistan. *Proc. Koninklijke Nederlandse Akad. Wetenschappen Ser. B* **84,** 71–99 (1981).
21. Cande, S. C. & Kent, D. V. Revised calibration of the geomagnetic polarity timescale for the late Cretaceous and Cenozoic. *J. Geophys. Res.* **100,** 6093–6095 (1995).
22. Berger, A., Loutre, M. F. & Laskar, J. Stability of the astronomical frequencies over the Earth's history for paleoclimate studies. *Science* **255,** 560–566 (1992).
23. Zhang, X. Y., Arimoto, R. & An, Z. S. Dust emission from Chinese desert sources linked to variations in atmospheric circulation. *J. Geophys. Res.* **102,** 28041–28047 (1997).
24. Wang, H. Z. (ed.) *Atlas of the Paleogeography of China* 121–123 (Cartographic, Beijing, 1985).

25. Chung, S. L. *et al.* Diachronous uplift of the Tibetan plateau starting 40 Myr ago. *Nature* **394,** 769–773 (1998).
26. Harrison, T. M., Copeland, P., Kidd, W. S. F. & Yin, A. Raising Tibet. *Science* **255,** 1663–1670 (1992).
27. Jansen, E. & Sjoholm, J. Reconstruction of glaciation over the past 6 Myr from ice-borne deposits in the Norwegian Sea. *Nature* **349,** 600–603 (1991).
28. Wolfe, J. A. in *The Carbon Cycle and Atmospheric CO_2: Natural Variations Archaean to Present* (eds Sundquist, E. T. & Broecker, W. S.) 357–375 (Monograph 32, American Geophysical Union, Washington DC, 1985).
29. Miller, K. G., Fairbanks, R. G. & Mountain, G. S. Tertiary oxygen isotope synthesis, sea level history, and continental margin erosion. *Paleoceanography* **2,** 1–19 (1987).
30. Rea, D. K., Snoeckx, H. & Joseph, L. H. Late Cenozoic eolian deposition in the North Pacific: Asian drying, Tibetan uplift, and cooling of the northern hemisphere. *Paleoceanography* **13,** 215–224 (1998).

Supplementary Information accompanies the paper on *Nature*'s website (http://www.nature.com).

Acknowledgements

We thank W. Wu, Z. Qiu, S. Zheng and Z. Qiu for the identification of micromammalian fossils, and Z.S. An, J. Guiot and R. Potts for discussions. This work is supported by the National Natural Science Foundation of China, the National Project for Basic Research on Tibetan Plateau, Chuangxin and Bairen Programs of the Chinese Academy of Sciences.

Correspondence and requests for materials should be addressed to Z.T.G. (e-mail: ztguo@95777.com).

Strong emission of methyl chloride from tropical plants

Yoko Yokouchi*, Masumi Ikeda*†, Yoko Inuzuka* & Tomohisa Yukawa‡

* *National Institute for Environmental Studies, 16-2 Onogawa, Tsukuba, Ibaraki 305-8506, Japan*
† *Meisei University, 2-1-1 Hodokubo, Hino, Tokyo 191-8506, Japan*
‡ *Tsukuba Botanical Garden, National Science Museum, 4-1-1 Amakubo, Tsukuba, Ibaraki 305-0005, Japan*

Methyl chloride is the largest natural source of ozone-depleting chlorine compounds, and accounts for about 15 per cent of the present atmospheric chlorine content[1]. This contribution was likely to have been relatively greater in pre-industrial times[2], when additional anthropogenic sources—such as chlorofluorocarbons—were absent. Although it has been shown that there are large emissions of methyl chloride from coastal lands in the tropics[3,4], there remains a substantial shortfall in the overall methyl chloride budget. Here we present observations of large emissions of methyl chloride from some common tropical plants (certain types of ferns and Dipterocarpaceae), ranging from 0.1 to 3.7 μg per gram of dry leaf per hour. On the basis of these preliminary measurements, the methyl chloride flux from Dipterocarpaceae in southeast Asia alone is estimated at 0.91 Tg yr^{-1}, which could explain a large portion of missing methyl chloride sources. With continuing tropical deforestation, natural sources of chlorine compounds may accordingly decrease in the future. Conversely, the abundance of massive ferns in the Carboniferous period[5] may have created an atmosphere rich in methyl chloride.

We studied CH_3Cl emissions from tropical plants in the lowland forest section (25 m × 20 m × 10–24 m high) of the Tropical Rainforest Glasshouse in Tsukuba Botanical Gardens, where more than 200 representative species from lowland tropical forests of southeast Asia grow. In order to see if tropical forests could be a significant source of CH_3Cl and to estimate the magnitude of the flux, CH_3Cl concentration in the glasshouse was measured over a few days in early September and mid October of 2000. During the experiment in October, air ventilation in the glasshouse was manually controlled to determine the accumulation of CH_3Cl. Air was sampled in the middle of the glasshouse from the observation catwalk (4 m high), as well as from outside, upwind of the glasshouse, by opening pre-evacuated canisters. CH_3Cl and some other volatile organic compounds were analysed with pre-concentration/capillary gas chromatography/mass spectrometry after samples were transported to the laboratory. Details of the analytical method have been published elsewhere[6,7].

Figure 1 shows the concentrations of CH_3Cl as well as carbonyl sulphide (COS), which is taken up by plants[8]. Ventilation status during the experiments is shown at the bottom of Fig. 1, along with the timings of the intentional (non-automatic) ventilation when the indoor atmosphere was entirely replaced with fresh outside air. CH_3Cl concentrations were always higher in the glasshouse (filled circles) than outside (open circles), and increased significantly when the windows were closed. Similar variations, but with smaller differences in concentration, were also observed for CH_3Br and CH_3I, clearly showing the emission of all these methyl halides from this tropical rainforest system. On the other hand, COS concentration was lower in the glasshouse; its variation was in strong contrast to that of CH_3Cl. The fluxes of CH_3Cl and COS were calculated from the averages of their accumulation rates (Δp.p.t.v. h^{-1}) under closed conditions and the dimensions of the glasshouse (20 m × 25 m × 17 m average height), giving 5.4 (3.8–8) μg m^{-2} h^{-1} for CH_3Cl and −0.28 (−0.11 to −0.3) μg m^{-2} h^{-1} for COS.

As a first step toward global extrapolation, the above CH_3Cl emission rate per unit area, 5.4 μg m^{-2} h^{-1} (or 47 mg m^{-2} yr^{-1}) was multiplied by the total area of tropical forest (1.73×10^{13} m^2; ref. 9), giving an annual emission of 0.82 Tg yr^{-1}. This estimate is expected to suffer from substantial uncertainty owing to the lower density and lower diversity of the plants in the glasshouse compared to those in actual tropical forests. Another extrapolation was done using the ratio of CH_3Cl emission to COS uptake in the glasshouse (100:5.2). By using the reported COS uptake by tropical forests (0.43 ± 0.10 Tg yr^{-1}; ref. 8), we calculated an annual CH_3Cl flux of 8.2 Tg yr^{-1}, a figure that exceeded even the total known sinks (3.5 Tg yr^{-1}; ref. 1). This estimate would not be affected by the difference in the density of plants, but would be revised downward if the ratio of CH_3Cl emission to COS uptake for tropical forests were lower. In any case, we may say that tropical forests are an important source of CH_3Cl on a global scale.

In order to determine which of the plants was responsible for the increase of CH_3Cl, or whether the soil was responsible, we measured flux by using an enclosure method. We chose 19 families (see Table 1) of plants from among the 55 families in the glasshouse

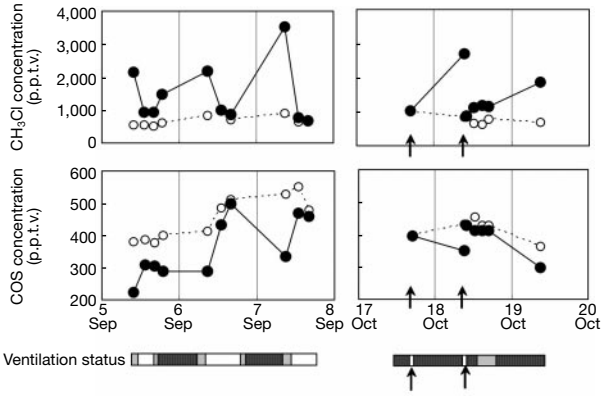

Figure 1 Atmospheric concentrations of CH_3Cl and COS during the observation periods, 5–8 September and 17–20 October. Filled circles, concentrations inside the Tropical Rainforest House; open circles, concentrations outside. Bar underneath time axis shows ventilation status: unshaded, windows mostly open; grey, windows partly open; black, windows mostly closed. Arrows under bar show times of intentional ventilation to replace the indoor atmosphere with fresh outside air. p.p.t.v., parts per trillion by volume.